EUROFUSION WPJET1-PR(16) 14719

KD Lawson et al.

Inclusion of molecular power loss terms in EDGE2D/EIRENE simulations of JET ITER-like wall L-mode discharges with comparisons of emission profiles

Preprint of Paper to be submitted for publication in
22nd International Conference on Plasma Surface Interactions
in Controlled Fusion Devices (22nd PSI)

This work has been carried out within the framework of the EUROfusion Consortium and has received funding from the Euratom research and training programme 2014-2018 under grant agreement No 633053. The views and opinions expressed herein do not necessarily reflect those of the European Commission.

P1.47

A study of the atomic and molecular power loss terms in EDGE2D-EIRENE simulations of JET ITER-like wall L-mode discharges

K D Lawson[a*], M Groth[b], D Harting[a], S Menmuir[a], D Reiter[c], S Brezinsek[c], G Corrigan[a], P Drewelow[d], C F Maggi[a], A G Meigs[a], J Simpson[a], M F Stamp[a], S Wiesen[c] & JET Contributors[1]

JET-EFDA, Culham Science Centre, Abingdon, OX14 3DB, UK

[a]*CCFE, Culham Science Centre, Abingdon, OX14 3DB, UK*

[b]*Aalto University, Otakaai 1, Espoo, 02150, Finland*

[c]*Forschungszentrum Jülich Gmbh, Institut für Energie- und Klimaforschung - Plasmaphysik, 52425 Jülich, Germany*

[d]*MPI für Plasmaphysik, 17491 Greifswald, Germany*

PACS: 52.25.Vy, 52.55.Fa, 52.55.Rk, 52.70.Kz

PSI-22 keywords: Divertor modelling, Divertor diagnostic, EDGE2D, JET, ILW

**Corresponding author address:* K1-1-40, Culham Science Centre, Abingdon, OX14 3DB, UK

**Corresponding author E-mail:* Kerry.Lawson@ukaea.uk

Presenting author: Kerry Lawson

Presenting author E-mail: Kerry.Lawson@ukaea.uk

[1] See the Appendix of F Romanelli *et al*, Proc. of the 25th IAEA Fusion Energy Conf. 2014, Saint Petersburg, Russia

Abstract

A discrepancy in the divertor radiated powers between EDGE2D-EIRENE simulations and JET-ILW experiments employing a set of NBI-heated L-mode discharges with step-wise density variation is investigated. The analysis shows the importance of the contributions from the deuterium fuel to the divertor radiated power, making these discharges ideal for this study.

Molecular radiation losses from D_2 molecules have been included for the first time and the present simulations allow the atomic and molecular electron power loss terms in EIRENE to be independently scaled in order to understand their importance in determining the simulated electron temperatures.

1. Introduction

An understanding of the behaviour of the plasma edge and divertor physics is essential for the design of next-step machines such as ITER, for which JET with its ITER-Like Wall (ILW) of Be in the main chamber and W in the divertor is ideally suited. Both fuel and edge impurities affect the power balance, thus determining the power reaching the divertor-target plates, which is limited by the mechanical and thermal properties of the plates. A study [1] of L-mode discharges during the present JET-ILW campaign and previous JET-C campaigns, in which the plasma-facing surfaces were C based materials (Carbon-Fibre Composite), has consistently shown a shortfall in the radiated power in the Scrape-Off Layer (SOL) and divertor calculated from EDGE2D-EIRENE simulations [2] below that measured by bolometry. A similar result is found for unseeded ELMy H-mode discharges by Järvinen *et al*. [3]. In order to gain understanding of this discrepancy, the contributions to the divertor radiated power (P_{rad}) as predicted by the simulations have been quantified and the results compared with measurements from bolometry for a density scan series of L-mode discharges run in JET-ILW. The simulations include for the first time molecular radiation losses from the D_2 molecules and allow the atomic and molecular power loss to the electrons to be independently scaled.

2. Simulations

The simulations of the JET-ILW, L-mode, NBI-heated discharges of Groth *et al*. [1] have been used to determine P_{rad} contributions (table 1). They apply to a density scan series of 2.5MA /

2.5T discharges (81472-81492) heated with 1.1, 1.2 or 1.6MW of NBI. The simulation geometry is taken from discharge 81472, the fuel being D with Be and W impurities. A range of outer midplane separatrix densities, $n_{e,sep}$, (7×10^{18} m^{-3} up to the maximum at which the simulations converge of 2-2.2$\times10^{19}$ m^{-3}) and of powers transported across the separatrix into the SOL (2.2 to 2.8 MW) was considered. Since little sensitivity to the power transported across the separatrix was found, only the 2.2 MW case is illustrated in this paper. The version of the EDGE2D-EIRENE code adapted to include D_2 and D_2^+ molecules was used and, for the first time here, molecular radiation losses from the D_2 molecules are included in the simulations. The full ITER reference atomic and molecular datasets were used as detailed by Kotov *et al.* [4]. To allow comparisons with the bolometric measurements, contributions to the radiated power are integrated along the diagnostic lines-of-sight (fig. 1). It was necessary to subtract a contribution of 1.3×10^4 W/m^2 from the bolometric signals to account for core radiation, although the D emission predominately comes from the divertor region.

3. Contributions to the divertor radiated power (P_{rad})

Table 1 details the contributions to the divertor P_{rad} and the importance of deuterium is evident, the impurities each accounting for no more than a few per cent [5]. These pulses therefore provide a stringent test of the simulations for the D fuel. Among the atomic D contributions, the largest component is due to D (Lyman) line radiation, in particular from the Ly_α line. P_{rad} due to free electron recombination, which for D is radiative recombination, can also be significant at temperatures less than ~1 eV (fig. 2). In these first simulations the number of D_2 and D_2^+ molecules was small, typically being ~10% and 3% of the number of D atoms, although significant variations from these values are seen in different regions of the divertor and as $n_{e,sep}$ increases. Lawson *et al.* [6] concluded that the simulated T_e tended to be too high in these simulations. Lowering T_e would result in higher atomic and molecular densities, which in turn

would lead to higher radiation, although this in part may be offset by falling excitation rates at the lower T_e.

4. Variation of the atomic and molecular electron power loss terms

The sensitivity of the simulations to the electron power loss terms was investigated by scaling these terms independently for the D atoms and D_2 molecules using a quadratic polynomial in T_e acting on the radiated power in the EIRENE code. The electron power loss due to the D atoms is

$$P_{e,loss}^{atoms} = 13.6 \times s_D + P_{D,line} \; eVm^3 s^{-1},$$

while that for the D_2 molecules is

$$P_{e,loss}^{molecules} = 15.4 \times s_{D_2} + 9.9 \times d_{D_2} + P_{D_2,electronic} \; eVm^3 s^{-1},$$

where *s* and *d* are the ionization and dissociation rate coefficients and *P* the power loss due to radiation, which for atoms is dominated by Ly_α and for molecules the Werner and Lyman band emission [7]. Figs. 2 and 3 compare atomic data from the AMJUEL [8] and ADAS [9] databases at two densities, $n_e=10^{19}$ and 10^{20} m^{-3}, fig. 2 illustrating the line power and radiative recombination rate coefficients and fig. 3 giving ratios of data from the two databases. Included in the latter are the D line power, $P_{D,line}$ (—, ...), the total power loss, $P_{e,loss}^{atoms}$ (----, -.-.-), ionization rates (with symbol +) and radiative recombination rates (×). Although ionization rates for the two databases show significant differences (fig. 3), this occurs at temperatures at which the contribution due to ionization is small, resulting in only small differences in the total power loss term. Fig. 4 illustrates the total (—) and radiative losses (----, -.-.-) for the D_2 molecules at $n_e=10^{19}$ and 10^{20} m^{-3}.

Four scalings of the atomic power loss term were tested:- 1) AMJUEL rates, 2) AMJUEL rates + 3%, 3) AMJUEL rates + 5% and 4) AMJUEL rates + 10%. The last corresponds to the expected accuracy of the electron collisional excitation rates, which largely determine the dominant line

power term, and it is noted that case 2 is most like the ADAS rates. The molecular behaviour is more complicated and a wider variation is explored:- 1) AMJUEL rates, 2) AMJUEL rates + 20% and 3) AMJUEL rates + 50%, all of which include molecular radiation losses.

An extreme sensitivity to the atomic power loss term is found in these new simulations, a small change in this term resulting in significantly lower electron temperatures and higher D_2 molecular densities. It should be emphasized that the four atomic cases considered are within the expected accuracy of the atomic data used. The sensitivity is illustrated in figs. 5 and 6, which show, respectively, the peak electron temperature at a height of z = -1.5 m in the outer divertor and the D_2 molecular density at the same radius for three $n_{e,sep}$, 1.4×10^{19} (symbol +), 1.5×10^{19} (×) and 1.8×10^{19} m-3 (*). The different lines in these figures correspond to the three molecular cases, 1 ——, 2 ---- and 3 -.-.-. The change was so marked between atomic cases 1 and 2 that additional simulations for the molecular case 1 at an $n_{e,sep}$ of 1.5×10^{19} m^{-3} have been made in order to increase the resolution at the lowest percentage change in atomic power loss term. Figure 7 illustrates the peak T_e at z=-1.5 m in the outer divertor (+ — +) and the peak T_e along the outer target plate (+ --- +). Looking for the peak T_e in the inner divertor usually led to flux surfaces that ended at the top of the inner divertor targets in the divertor throat. Consequently, it was thought more representative to compare the data at the same position in the inner divertor. T_e on the inner divertor target plate at R=2.42, z = -1.54 m (×---×) and in the inner divertor volume at R= 2.46, z=-1.5 m (×—×) are illustrated.

The effect on the initial simulations of including the molecular radiation can be seen in the reconstruction of the bolometric profiles (figs. 8 to 10) for the three $n_{e,sep}$ already illustrated and is seen to be small at the lowest $n_{e,sep}$, but more significant at higher $n_{e,sep}$, (+---+ without and + — + with the D_2 molecular radiation). This is explained by the comparatively small number of D_2 molecules in the initial simulations at low $n_{e,sep}$. In contrast, increasing the atomic power loss

term (×—×) results in a marked change at all densities, affecting the inner / outer divertor balance of the P_{rad} profile and tending to broaden the radiation features, the new simulations better reflecting the overall profile of the bolometric measurements. Since there can be a significant variation in the measured profiles, four profiles (without symbols, in black) are illustrated in these figures. Varying the molecular power loss term has the greatest effect in atomic case 1 at high $n_{e,sep}$. It is noted that modifying the molecular power loss term alone would not allow the lowest temperatures found in these simulations to be reached. Despite the improvement in the profile shape a P_{rad} deficit still remains.

5. Conclusions

Comparisons between EDGE2D-EIRENE simulations and measurements of P_{rad} in a density scan series of L-mode, NBI-heated discharges emphasize the importance of atomic and molecular D in determining the radiated power. Independent scalings of the atomic and molecular electron power loss terms have been used to gain understanding of a shortfall in the simulated radiated power compared with bolometric measurements. An extreme sensitivity to the atomic power loss term, in particular, is found which allows a lower temperature parameter space to be accessed, with improved radiation profiles, although still with a deficit in the divertor radiated power. Inclusion of molecular radiation losses from the D_2 molecules had a small effect on the initial low density simulations, becoming more important with increasing $n_{e,sep}$ with their lower temperatures and higher molecular densities. The new parameter space will be exploited in the first instance by extending the analysis of the L-mode regime with comparisons of line radiation profiles and molecular densities and in the longer term will be tested in other regimes.

Acknowledgements

This work has been carried out within the framework of the EUROfusion Consortium and has received funding from the Euratom research and training programme 2014-2018 under grant agreement No. 633053 and from the RCUK Energy Programme [grant no. EP/I501045]. To obtain further information on the data and models underlying this paper please contact PublicationsManager@ukaea.uk. The views and opinions expressed herein do not necessarily reflect those of the European Commission.

References

[1] Groth *et al*., Nucl. Fusion **53** (2013) 093016

[2] Wiesen, EDGE2D/EIRENE code interface report, JET ITC-Report, http://www.eirene.de/e2deir_report_30jun06.pdf, 2006

[3] Järvinen *et al*., J. Nuc. Mater. **463** (2015) 135

[4] Kotov *et al*., PPCF **50** (2008) 105012

[5] Brezinsek *et al*., J. Nuc. Mater. **438** (2013) S303

[6] Lawson *et al*., J. Nuc. Mater. **463** (2015) 582

[7] Terry, J. Vac. Sci. Technol. **A1** (1983) 831

[8] Reiter, http://www.eirene.de/html/a_m_data.html, 2016

[9] Summers, The ADAS User Manual, version 2.6, http://adas.phys.strath.ac.uk, 2004

Table 1. Contributions to the divertor radiated power (P_{rad}).

Contributions to the radiated power	
Line radiation from D.	Ly_α ~85-90%, Ly_β ~10% and other lines ~3%.
D line radiation due to recombination directly populating excited D atomic levels.	$<10^{-5}$ of D line radiation.
Line radiation from D_2 molecules.	~10% of D line radiation.
Line radiation from D_2^+ molecules.	~3% of D line radiation.
Radiative recombination to D followed by cascading within D atoms + Bremsstrahlung.	$<10^{-2}$ at low $n_{e,sep}$, rising to ~30% at high $n_{e,sep}$.
Be impurity radiation.	Variable - few % in cases considered.
Estimated P_{rad} contributions	
C and O impurity radiation.	Variable - similar to Be.
High Z impurity (Ni, Cu and W) line radiation.	Generally smaller than low Z elements at the low T_e of the divertor.

Figure Captions

Figure 1. Lines-of-sight of the bolometer.

Figure 2. D line power and radiative recombination rate coefficients, AMJUEL —— $n_e=10^{19}m^{-3}$, ... $n_e=10^{20}m^{-3}$, ADAS - - - $n_e=10^{19}m^{-3}$, -.-.- $n_e=10^{20}m^{-3}$.

Figure 3. Ratio of ADAS to AMJUEL rates, D line power —— $n_e=10^{19}m^{-3}$, ... $n_e=10^{20}m^{-3}$, total power loss - - - $n_e=10^{19}m^{-3}$, -.-.- $n_e=10^{20}m^{-3}$, ionization + — + $n_e=10^{19}m^{-3}$, + --- + $n_e=10^{20}m^{-3}$, radiative recombination ×—× $n_e=10^{19}m^{-3}$, ×---× $n_e=10^{20}m^{-3}$.

Figure 4. Total D_2 power loss —— $n_e=10^{19}m^{-3}$, $n_e=10^{20}m^{-3}$, D_2 radiative loss - - - $n_e=10^{19}m^{-3}$, -.-.- $n_e=10^{20}m^{-3}$, data from AMJUEL.

Figure 5. Maximum T_e in the outer divertor at z = -1.5 m as a function of the change in the atomic power loss term. + $n_{e,sep}=1.4\times10^{19}$ m^{-3}, × $n_{e,sep}=1.5\times10^{19}$ m^{-3}, * $n_{e,sep}=1.8\times10^{19}$ m^{-3}. —— molecular case 1, - - - molecular case 2, -.-.- molecular case 3. All simulations have 2.2 MW power to SOL.

Figure 6. D_2 density at position of maximum T_e in the outer divertor at z = -1.5 m as a function of the change in the atomic power loss term. + $n_{e,sep}=1.4\times10^{19}$ m^{-3}, × $n_{e,sep}=1.5\times10^{19}$ m^{-3}, * $n_{e,sep}=1.8\times10^{19}$ m^{-3}. —— molecular case 1, - - - molecular case 2, -.-.- molecular case 3. All simulations have 2.2 MW power to SOL.

Figure 7. Maximum T_e in the outer divertor at z = -1.5 m, + — +, and on the outer target, + --- +, as a function of the change in the atomic power loss term for molecular case 1 with $n_{e,sep}=1.5\times10^{19}$ m^{-3}. For the inner divertor, T_e is shown at a fixed position, R=2.42 m, z=-1.54 m on the inner target, ×---×, and R=2.46 m, z=-1.50 m, in the inner divertor volume, ×—× for the same case. All simulations have 2.2 MW power to SOL.

Figure 8. Bolometric profiles for pulse 81480 at ~ 17 s, $n_{e,sep} = 1.4\times10^{19}$ m^{-3}. Measured data, 4 curves without symbols (in black), 1.3×10^{4} W/m^2 core emission subtracted. + --- + initial simulation, + — + with D_2 molecular radiation, ×—× scaled atomic case 2 and molecular case 3 with D_2 molecular radiation. All simulations have 2.2 MW power to SOL.

Figure 9. Bolometric profiles for pulse 81472 at ~ 13 s, $n_{e,sep} = 1.5\times10^{19}$ m^{-3}. Measured data, 4 curves without symbols (in black), 1.3×10^{4} W/m^2 core emission subtracted. + --- + initial simulation, + — + with D_2 molecular radiation, ×—× scaled atomic case 4 and molecular case 2 with D_2 molecular radiation. All simulations have 2.2 MW power to SOL.

Figure 10. Bolometric profiles for pulse 81472 at ~ 16 s, $n_{e,sep} = 1.8\times10^{19}$ m^{-3}. Measured data, 4 curves without symbols (in black), 1.3×10^{4} W/m^2 core emission subtracted. + --- + initial simulation, + — + with D_2 molecular radiation, ×—× scaled atomic case 4 and molecular case 1 with D_2 molecular radiation. All simulations have 2.2 MW power to SOL.

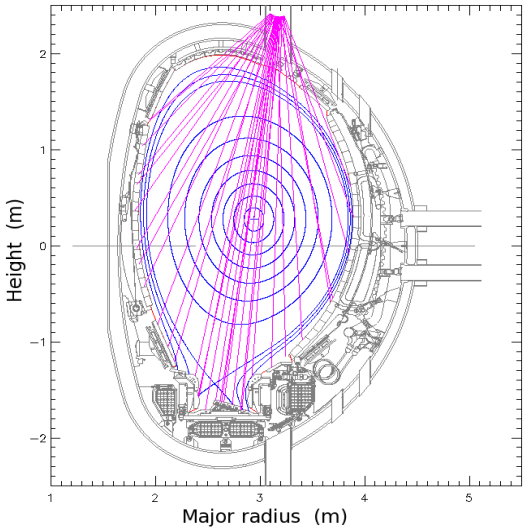

Figure 1.

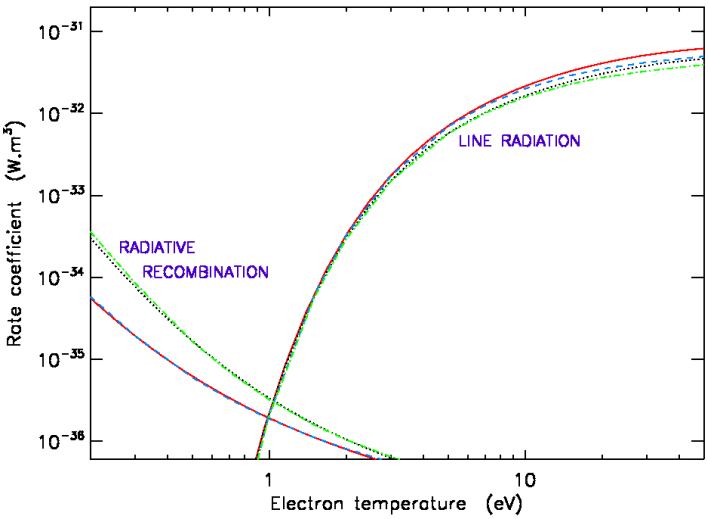
Rate coefficient (W.m^3)
10^{-31}
10^{-32}
10^{-33}
10^{-34}
10^{-35}
10^{-36}
LINE RADIATION
RADIATIVE
RECOMBINATION
1
10
Electron temperature (eV)

Figure 2.

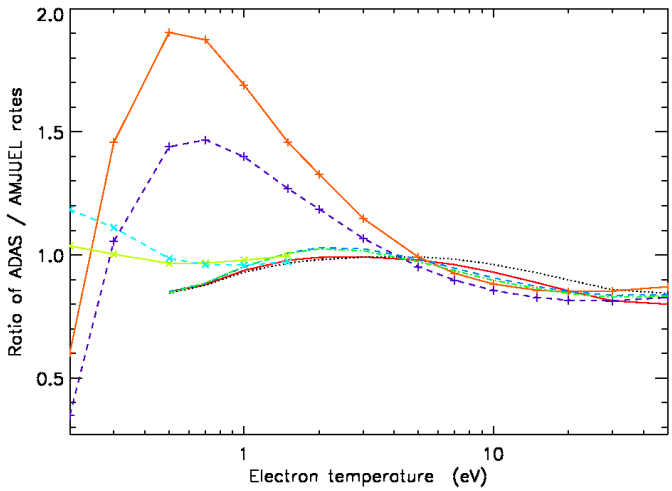
2.0
1.5
1.0
0.5
Ratio of ADAS / AMJUEL rates
1
10
Electron temperature (eV)

Figure 3.

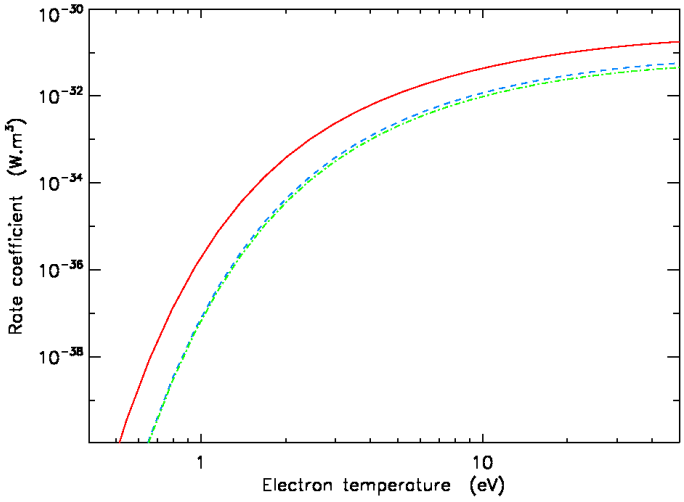
10^-30
10^-32
10^-34
10^-36
10^-38
Rate coefficient (W.m^3)
1
10
Electron temperature (eV)

Figure 4.

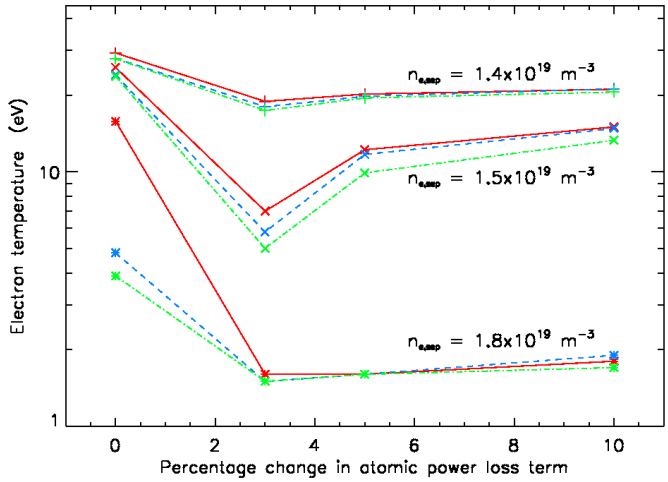
Electron temperature (eV)
10
1
0
2
4
6
8
10
Percentage change in atomic power loss term
$n_{e,sep}$ = 1.4x10^{19} m^{-3}
$n_{e,sep}$ = 1.5x10^{19} m^{-3}
$n_{e,sep}$ = 1.8x10^{19} m^{-3}

Figure 5.

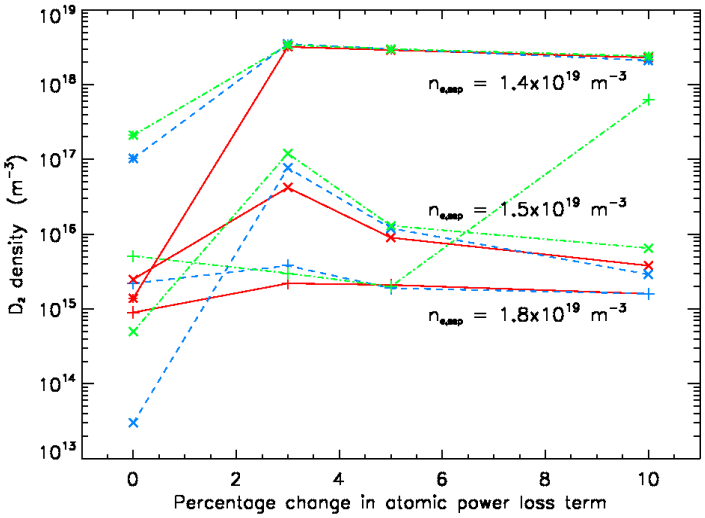
10^{19}
10^{18}
10^{17}
10^{16}
10^{15}
10^{14}
10^{13}
D_2 density (m^{-3})
$n_{e,sep}$ = 1.4x10^{19} m^{-3}
$n_{e,sep}$ = 1.5x10^{19} m^{-3}
$n_{e,sep}$ = 1.8x10^{19} m^{-3}
0
2
4
6
8
10
Percentage change in atomic power loss term

Figure 6.

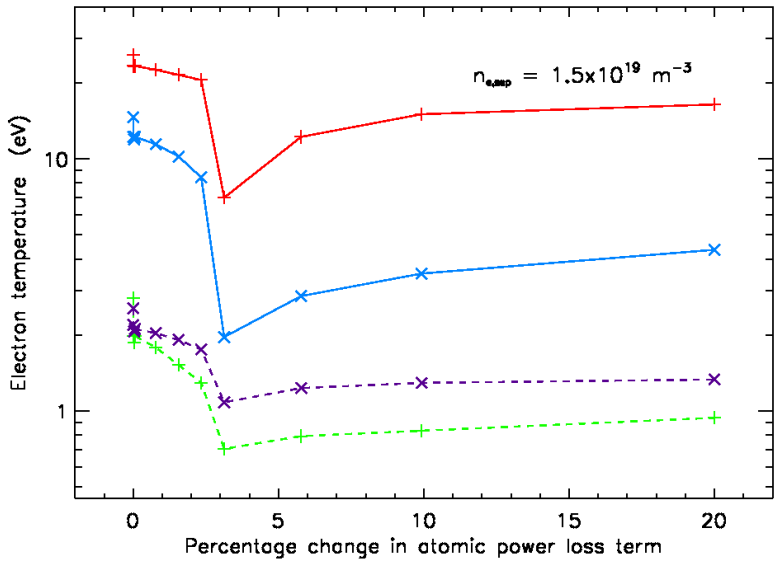
$n_{e,sep}$ = 1.5x10^{19} m^{-3}
Electron temperature (eV)
10
1
0
5
10
15
20
Percentage change in atomic power loss term

Figure 7.

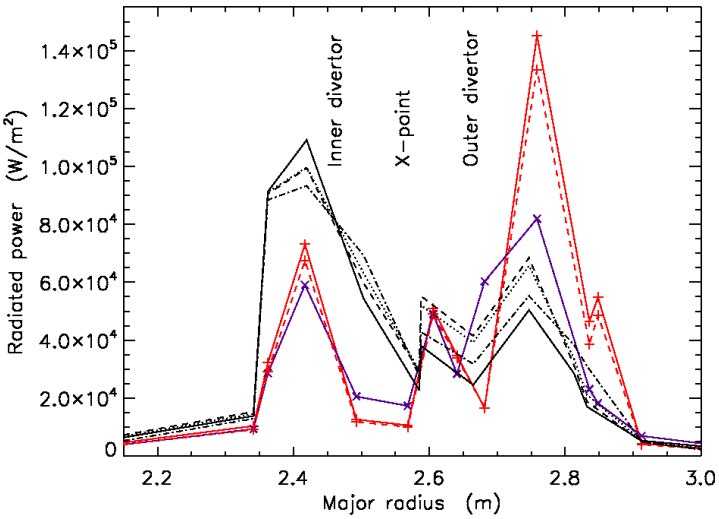
Radiated power (W/m²)
1.4×10⁵
1.2×10⁵
1.0×10⁵
8.0×10⁴
6.0×10⁴
4.0×10⁴
2.0×10⁴
0
2.2
2.4
2.6
2.8
3.0
Major radius (m)
Inner divertor
X-point
Outer divertor

Figure 8.

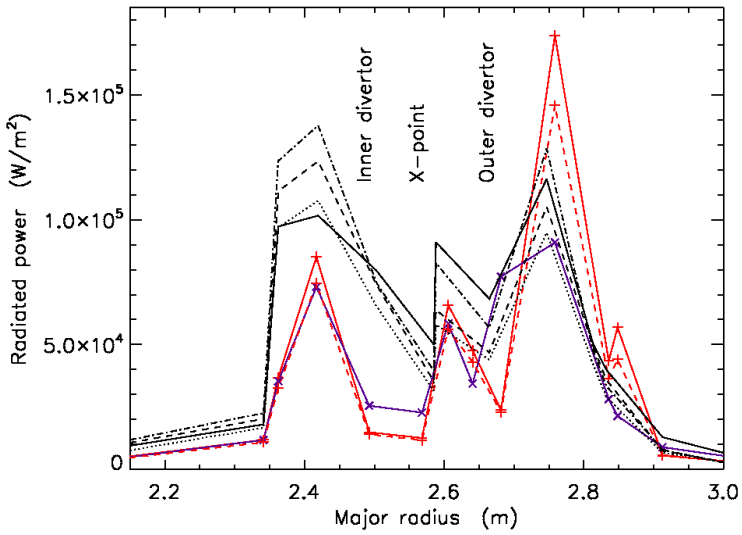
Radiated power (W/m²)
1.5×10⁵
1.0×10⁵
5.0×10⁴
0
Inner divertor
X-point
Outer divertor
2.2
2.4
2.6
2.8
3.0
Major radius (m)

Figure 9.

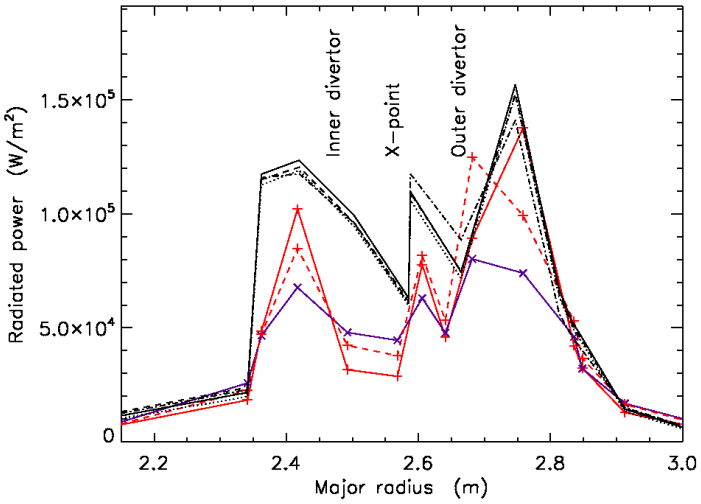
Inner divertor
X−point
Outer divertor
Radiated power (W/m²)
1.5×10⁵
1.0×10⁵
5.0×10⁴
0
2.2
2.4
2.6
2.8
3.0
Major radius (m)

Figure 10.